Interfacial engineering of cobalt sulfide/graphene hybrids for highly efficient ammonia electrosynthesis

Pengzuo Chen[a,b,c,1], Nan Zhang[d,1], Sibo Wang[a,b,c], Tianpei Zhou[a,b,c], Yun Tong[a,b,c], Chengcheng Ao[d], Wensheng Yan[d], Lidong Zhang[d], Wangsheng Chu[d], Changzheng Wu[a,b,c,2], and Yi Xie[a,b,c]

[a]Hefei National Laboratory for Physical Science at the Microscale, University of Science and Technology of China, Hefei, 230026 Anhui, People's Republic of China; [b]Collaborative Innovation Center of Chemistry for Energy Materials, University of Science and Technology of China, Hefei, 230026 Anhui, People's Republic of China; [c]Chinese Academy of Sciences Key Laboratory of Mechanical Behavior and Design of Materials, University of Science and Technology of China, Hefei, 230026 Anhui, People's Republic of China; and [d]National Synchrotron Radiation Laboratory, University of Science and Technology of China, Hefei, 230029 Anhui, People's Republic of China

Edited by Peidong Yang, University of California, Berkeley, Lawrence Berkeley National Laboratory, Berkeley, CA, and approved February 14, 2019 (received for review October 19, 2018)

Electrocatalytic N_2 reduction reaction (NRR) into ammonia (NH_3), especially if driven by renewable energy, represents a potentially clean and sustainable strategy for replacing traditional Haber–Bosch process and dealing with climate change effect. However, electrocatalytic NRR process under ambient conditions often suffers from low Faradaic efficiency and high overpotential. Developing newly regulative methods for highly efficient NRR electrocatalysts is of great significance for NH_3 synthesis. Here, we propose an interfacial engineering strategy for designing a class of strongly coupled hybrid materials as highly active electrocatalysts for catalytic N_2 fixation. X-ray absorption near-edge spectroscopy (XANES) spectra confirm the successful construction of strong bridging bonds (Co–N/S–C) at the interface between CoS_x nanoparticles and NS-G (nitrogen- and sulfur-doped reduced graphene). These bridging bonds can accelerate the reaction kinetics by acting as an electron transport channel, enabling electrocatalytic NRR at a low overpotential. As expected, CoS_2/NS-G hybrids show superior NRR activity with a high NH_3 Faradaic efficiency of 25.9% at −0.05 V versus reversible hydrogen electrode (RHE). Moreover, this strategy is general and can be extended to a series of other strongly coupled metal sulfide hybrids. This work provides an approach to design advanced materials for ammonia production.

interfacial engineering | general strategy | cobalt sulfides | bridging bonds | NH_3 electrosynthesis

Ammonia is not only regarded as a promising chemical hydrogen storage candidate due to its high energy density but also an important raw material for the fertilizer, pharmaceutical, and light industries (1–3). Currently, industrial NH_3 synthesis still relies on the traditional Haber–Bosch process, which must be performed at high temperatures (350∼550 °C) and high pressures (150∼350 atm) with high-purity streams of nitrogen and hydrogen as raw materials (4, 5). This process accounts for 1∼3% of global annual energy production and represents a significant contributor to climate change (6, 7). Thus, there is an urgent need to explore new technologies for green and efficient NH_3 synthesis. The electrochemical N_2 reduction reaction (NRR) enables NH_3 synthesis using N_2 and H_2O under ambient conditions, making it a highly promising candidate for clean, carbon-free, and sustainable NH_3 production (8, 9). However, the sluggish kinetics of N_2 absorption and the permanent dipole of the triple bond seriously impede its catalytic efficiency (10). Therefore, the discovery of low-cost and highly efficient NRR catalysts for NH_3 electrosynthesis is of great significance.

To date, a series of noble metal [Au (11, 12), Pd (13, 14), Ru (15, 16)] and nonnoble metal electrocatalysts [metal oxides (17, 18), sulfides (19), nitrides (20, 21), and heteroatom-doped carbon materials (22–24)] has been pursued for NRR. However, these catalysts still suffer from low NH_3 yield and selectivity due to the small number of catalytically active sites and poor charge-transport capacity (11, 25, 26) Recently, interfacial engineering by combining electrocatalysts with hierarchical substrates such as TiO_2, graphene, and CeO_2 nanofibers has been regarded as an efficient way to protect growing nanoparticles from agglomeration and supply more active sites, thereby enhancing NRR catalytic activity (11, 14, 25). However, most of these hybrid catalysts lack strongly coupled bonds at the interface between the substrates and electrocatalysts, which still severely limits their interfacial charge-transfer capacity, restricting the scope of promoting the electrocatalytic activity for NRR.

Recently, numerous regulating strategies, such as designing 2D/2D hybrid materials to improve the contact interface (27) or directly constructing strong bridging bonds between nanoparticles and supports (28), have been applied in developing highly active catalysts for oxygen evolution and reduction. Among these strategies, the construction of strong bridging bonds at an interface would be a more effective way to improve catalytic activity because these bonds can directly accelerate reaction kinetics by functioning as an electron transport channel. Herein, we highlight an interfacial engineering strategy for strongly coupled hybrid materials as highly active NRR electrocatalysts. Remarkably, the strong Co–N/S–C bridging bonds enable a controllable interfacial

Significance

Ammonia is one of the most important chemical raw materials with an annual production exceeding 200 million tons. The Haber–Bosch process is still the dominant route for industrial ammonia synthesis, which consumes 1∼3% of global annual energy production and represents a significant contributor to climate change. Electrocatalytic N_2 reduction reaction is an attractive alternative candidate for carbon-free and sustainable NH_3 production, but often suffers from low efficiency. Here, we developed an interfacial engineering strategy for preparing a class of strongly coupled hybrid electrocatalysts for N_2 fixation. The hybrids exhibit superior N_2 reduction reaction activity with a high NH_3 Faradaic efficiency of 25.9% under ambient conditions. This strategy provides an approach to design advanced materials for ammonia production.

Author contributions: C.W. designed research; P.C., N.Z., and C.W. performed research; C.A., W.Y., L.Z., and W.C. contributed new reagents/analytic tools; P.C., N.Z., S.W., T.Z., Y.T., C.A., W.Y., L.Z., and W.C. analyzed data; and P.C., N.Z., C.W., and Y.X. wrote the paper.

The authors declare no conflict of interest.

The authors declare no competing financial interests.

This article is a PNAS Direct Submission.

[1]P.C. and N.Z. contributed equally to this work.

[2]To whom correspondence should be addressed. Email: czwu@ustc.edu.cn.

This article contains supporting information online at www.pnas.org/lookup/suppl/doi:10.1073/pnas.1817881116/-/DCSupplemental.

Published online March 14, 2019.

coupling effect between the cobalt sulfide nanoparticles and graphene. As expected, the strong-coupled CoS_2/NS-G catalyst exhibits excellent NRR performance with a high NH_3 yield rate (25.0 μg h^{-1}·mg^{-1}_{cat} at −0.2 V vs. RHE) and Faradaic efficiency (25.9% at −0.05 V vs. RHE) under ambient conditions. Moreover, a series of other strongly coupled hybrid materials (MS_x/NS-G; M = Ni, Fe, and Sn; $x = 1, 2$) was also developed for NRR by using this general approach. This work paves a route for developing advanced electrocatalysts for ammonia synthesis.

Results and Discussion

Characterizations of CoS_x/NS-G Hybrid Materials. In this work, strong-coupled CoS_x/NS-G hybrids were synthesized by an in situ annealing method that enables the uniform growth of cobalt sulfides nanoparticles on a graphene sheet. The stoichiometric ratio of CoS_2 to CoS can be easily regulated by controlling the amount of thiourea powder added (*SI Appendix*, Fig. S1). The detailed structural features of the products were investigated by X-ray diffraction (XRD). All of the different diffraction peaks can be well indexed to standard cubic CoS_2 [Joint Committee on Powder Diffraction Standards (JCPDS) card no. 70–2866] and hexagonal CoS (JCPDS card no. 70–2864) without any peaks for impurities, indicating the successful preparation of different phases of CoS_2 and CoS samples (*SI Appendix*, Fig. S3). Moreover, transmission electron microscopy (TEM) and high-resolution TEM (HRTEM) were further conducted to evaluate the morphology and composition of the CoS_2/NS-G and CoS/NS-G samples. As shown in Fig. 1*A* and *SI Appendix*, Fig. S4*A*, both the as-prepared CoS_2 and CoS sample have morphologies of small nanoparticles uniformly grown on the graphene sheet. The size distribution of the resulting CoS_2 nanoparticles was also characterized. As shown in *SI Appendix*, Fig. S17 *C* and *D*, most sulfide nanoparticles are between 20 and 60 nm. The metallic nanoparticles can also been tuned by employing different amounts of cobalt salt as raw material. *SI Appendix*, Fig. S17 shows TEM images and particle-size distribution of CoS_2/NS-G hybrids synthesized by different amounts of cobalt salt. CoS_2/NS-G synthesized by 0.1, 0.2, and 0.4 mmol $CoCl_2$ exhibit particle size of 10–30, 20–60, and 100–250 nm, respectively. The above result reveals that the particle size of the cobalt sulfide increases with the increasing of the adding amount of cobalt salt, and the composition of metallic nanoparticles can be tuned by controlling the synthetic raw material. Moreover, the HRTEM image shows a lattice fringe of 3.2 Å (Fig. 1*A*, *Inset*), which is consistent with the (111) lattice plane of cubic CoS_2, while the (002) plane of the hexagonal CoS sample can also be identified by clear lattice fringes of 2.6 Å (*SI Appendix*, Fig. S4*B*). Furthermore, energy-dispersive X-ray spectroscopy elemental mapping analysis of CoS_2/NS-G and CoS/NS-G shows the homogeneous distribution of Co, C, N, and S in the as-prepared hybrids (Fig. 1*B* and *SI Appendix*, Fig. S6*B*), indicating the successful introduction of N and S into the graphene.

X-ray photoelectron spectroscopy (XPS) was carried out to investigate the compositions and valence states of CoS_2/NS-G and CoS/NS-G. The core-level scan XPS spectra of Co 2p, as illustrated in Fig. 1*C*, comprise two main peaks that result from the spin–orbit splitting of the p orbital and are assigned to Co $2p_{3/2}$ and Co $2p_{1/2}$ (29, 30). The two satellite peaks located at ∼786.8 and 803.7 eV can be ascribed to the shakeup type peaks of Co (31). In the high-resolution XPS spectra of S 2p shown in Fig. 1*D*, the CoS_2/NS-G sample exhibits two main peaks located at 162.9 and 164.1 eV that can be attributed to S $2p_{3/2}$ and S $2p_{1/2}$, indicating the presence of $(S_2)^{2-}$-type species bonded to Co^{2+} (32, 33). In contrast, these two peaks are slightly shifted to lower binding energies of 161.9 and 163.2 eV for the CoS/NS-G sample, which is consistent with the bonding energies of S^{2-} species (34). The different valence bonds in the sulfur spectra further demonstrate the successful preparation of two phases of cobalt sulfide. The peaks at 165.3 eV for the two hybrids can be ascribed to the C–S–C bond, indicating the introduction of S into the graphene (35, 36). Moreover, *SI Appendix*, Fig. S7 shows that the core-level scan spectrum of N 1s can be divided into several characteristic peaks located at 398.6, 400.0, and 401.6 eV, which

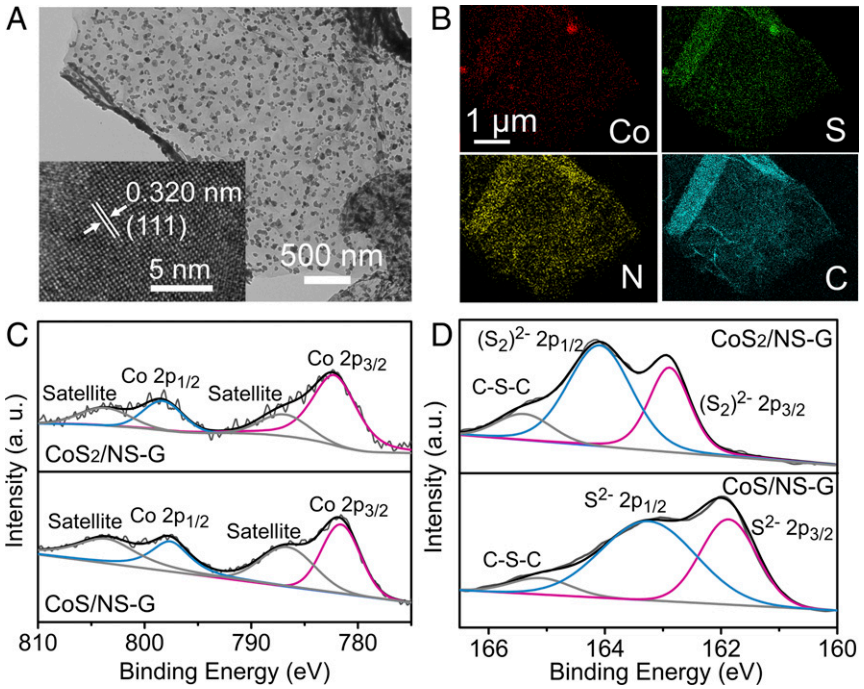

Fig. 1. Characterization of CoS_x/NS-G hybrids. (*A*) TEM image and corresponding HRTEM image (*Inset*) of CoS_2/NS-G. (*B*) Elemental mapping images of the CoS_2/NS-G hybrid. High-resolution XPS spectra of Co 2p (*C*) and S 2p (*D*) for the CoS_2/NS-G and CoS/NS-G hybrid products.

can be attributed to the peaks of pyridinic-N, pyrrolic-N, and graphitic-N, respectively (37, 38).

Characterizations of Interfacial Interaction. To gain insight into the interfacial interaction, synchrotron soft X-ray absorption near-edge spectroscopy (XANES), which is sensitive to local chemical configuration and partial electronic state, was also performed. As shown in Fig. 2*A*, the cobalt L-edge XANES spectra of CoS_2/NS-G and CoS/NS-G exhibit two main peaks located at energies of 772.5 and 787.5 eV, respectively, corresponding to the L_3- and L_2 edges. The enhanced absorption intensity and the increased resolution of the XANES features of CoS_2/NS-G are in accordance with the typical characteristics of standard CoS_2 and CoS samples (39, 40). Furthermore, the sulfur L-edge XANES spectra (Fig. 2*B*) of CoS_2/NS-G and CoS/NS-G show obvious peaks in the region of 163~168 eV corresponding to C–S–C coordination species, which are consistent with the result of the NS-G sample (35, 41). This result suggests that there is substantial S doping into the graphene in both hybrid materials.

In Fig. 2*C*, the carbon K-edge spectra of the three materials all are dominated by three strong resonances with peak centers of ~284.2 eV (peak C1), 286.9 eV (peak C2), and 291.2 eV (peak C3). These resonances can be ascribed to the dipole transition of the 1s core electron of carbon into the $\pi^*_{C=C}$, $\pi^*_{C-O/N/S-C}$, and σ^*_{C-C} antibonding states, respectively, consistent with previous reports (42). The preservation of the main features indicates that the cobalt sulfide nanoparticles did not change the framework of the NS-G support. However, the different types of cobalt sulfide subtly modified the electronic state and the chemical bond of the corresponding hybrid materials, as indicated by the intensity changes in peaks C1 and C2. The intensity decrease in peak C1 suggests that the $\pi^*_{C=C}$ unfilled state of the aromatic ring was doped by exotic electrons, while the sharp intensity increase in peak C2 confirms that additional strong chemical bonds form out of the graphene layer and hence introduce more sp^3 interactions (28, 43). This result provides solid evidence to confirm that numerous Co–N/S–C bonds existed at the interface between the nanoparticles and graphene of the CoS_2/NS-G and CoS/NS-G hybrids and that charge transfer from cobalt to the N,S-decorated graphene occurred. This can be further confirmed by the double peaks within the energy range from 294 to 300 eV, which are characteristic of an sp^3 interaction in carbon-based materials. Moreover, to further characterize the extent of the interfacial interactions, the normalized intensities of peak C1 and C2 relative to C3 are shown in *SI Appendix*, Table S1. Compared with CoS/NS-G, CoS_2/NS-G exhibits an increased intensity ratio of C2/C3 and a more obvious sp^3 interaction, which demonstrates that a stronger interfacial interaction was constructed in CoS_2/NS-G and would enable superior charge transfer ability for electrocatalysis. In addition, the cobalt sulfide nanoparticles not only regulate the electronic state of the aromatic ring but also selectively control the nitrogen configurations in the hybrid materials, which can be further confirmed by the nitrogen K-edge XANES spectra (Fig. 2*D*). According to previous research works (28), nitrogen XANES features arise from two types of nitrogen chemical configurations: C-*N*-C and *N*-3C. The former, which features in the energy region of 395–400 eV, indicates the chemical states of the nitrogen from pyridinic ring and pyrrolic ring; the latter, a peak at ~405 eV, denotes graphitic nitrogen. The almost identical *N*-3C features of the CoS_2/NS-G and NS-G hybrids and the obviously varying C-*N*-C features suggest that the introduction of CoS_2 nanoparticles maintained the frame structure of the N,S-doped graphene and modified the nitrogen configurations in the edge cutting. Therefore, a strong interfacial interaction was successfully constructed in the as-prepared hybrid materials, which favors the electrocatalytic activity for NRR.

Electrocatalytic Activity for NRR. To study the NRR catalytic activity of CoS_2/NS-G and CoS/NS-G, electrocatalytic N_2 reduction measurements were carried out in an Ar- or N_2-saturated 0.05 M H_2SO_4 solution under ambient conditions. As shown in Fig. 3*A*,

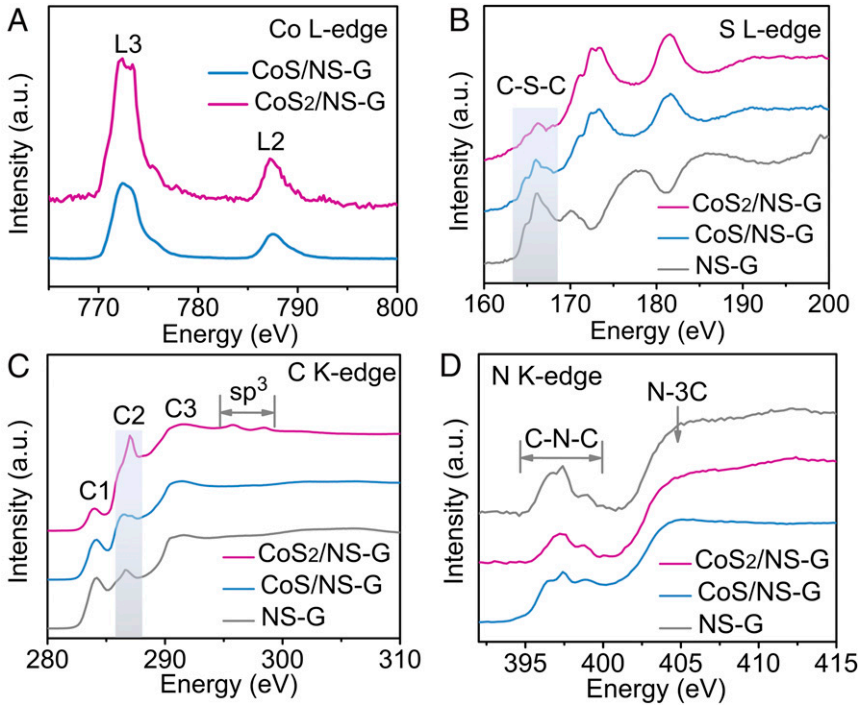

Fig. 2. Local chemical configuration and electronic state of CoS_x/NS-G hybrid catalysts. (*A*) Co L-edge XANES spectra of the CoS/NS-G and CoS_2/NS-G hybrids. S L-edge (*B*), C K-edge (*C*), and N K-edge (*D*) XANES spectra of CoS/NS-G, CoS_2/NS-G, and NS-G materials.

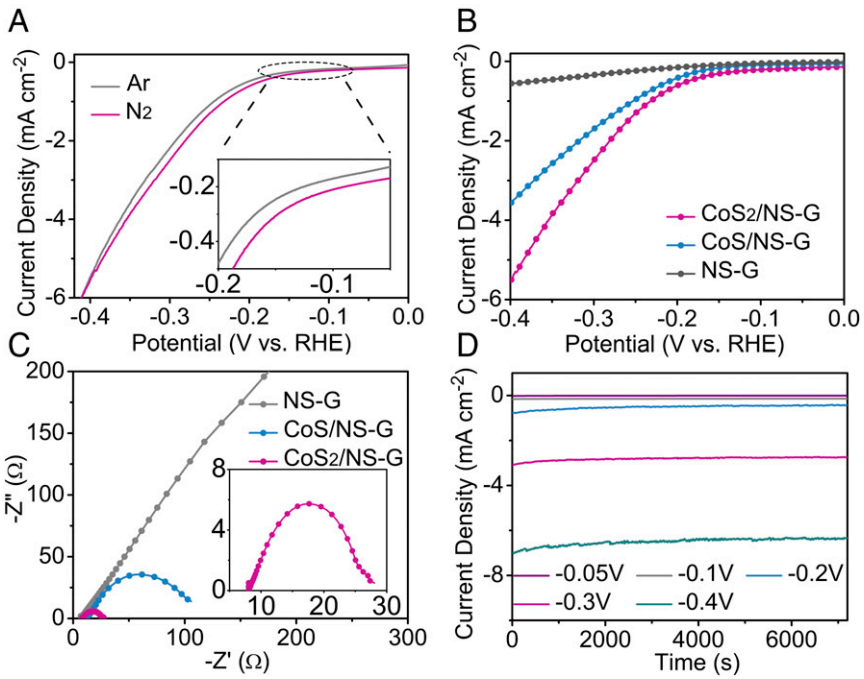

Fig. 3. Electrochemical characterization of CoS_x/NS-G hybrids. (*A*) Linear sweep voltammetry tests of CoS_2/NS-G in Ar- and N_2-saturated 0.05 M H_2SO_4 under ambient conditions. Polarization curves (*B*) and corresponding Nyquist plots (*C*) of different catalysts in N_2-saturated 0.05 M H_2SO_4 solution. (*D*) Chronoamperometric results of the CoS_2/NS-G hybrid at the different potentials.

NRR is initiated at −30 mV versus RHE under N_2 saturation at room temperature and atmospheric pressure, which is different from that in Ar. The obvious difference in current density between N_2- or Ar-saturated environments can also be observed at a more positive potential, suggesting the high NRR catalytic activity of the CoS_2/NS-G catalysts. Moreover, the polarization curves of the CoS_2/NS-G hybrid exhibit a more positive onset potential (−30 mV) and higher current density than those of CoS/NS-G (−45 mV) and NS-G (−95 mV), which can be attributed to the CoS_2/NS-G hybrid having the strongest interfacial coupling effect (Fig. 3*B*). Electrochemical impedance spectroscopy analysis of the CoS_2/NS-G catalyst also exhibits that its

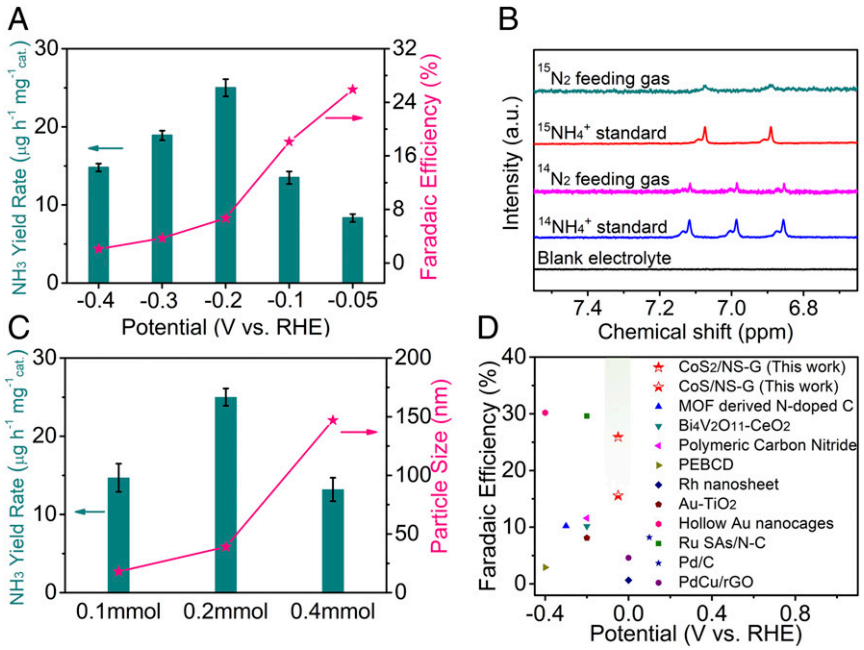

Fig. 4. Catalytic performance of CoS_x/NS-G during the electrocatalytic N_2 reduction process. (*A*) NH_3 yield rate and Faradaic efficiency of CoS_2/NS-G at each given potential. (*B*) NMR spectra of ^1H for the electrolytes after NRR test by using $^{15}N_2$ and $^{14}N_2$ as feeding gas. (*C*) Comparison of NH_3 yield rate at −0.2 V and particle size for CoS_2/NS-G hybrids which was synthesized by different amounts of cobalt salt. (*D*) Faradaic efficiency of well-developed NRR electrocatalysts at room temperature and atmospheric pressure (*SI Appendix*, Table S2).

charge-transfer resistance is smaller than that of CoS/NS-G and NS-G (Fig. 3*C*), indicating that strong Co–N/S–C bonds lead to faster reaction kinetics by accelerating electron transfer. In addition, the current density at different potentials shows good stability (Fig. 3*D*). As shown in *SI Appendix*, Fig. S18, the current density exhibits little degeneration for CoS_2/NS-G after chronoamperometric test of 10 h. These result confirms that CoS_2 hybrid shows good stability in N_2-saturated 0.05 M H_2SO_4 during NRR test, which might be attributed to the good dispersion of the cobalt sulfide nanoparticles on NS-G support and the strongly coupled interaction between them.

To further verify the NRR activity of the CoS_2/NS-G and CoS/NS-G hybrid catalysts, a chronoamperometric method was employed to investigate the NH_3 yield rate and Faradaic efficiency. As shown in Fig. 4*A*, the CoS_2/NS-G hybrid shows a high yield rate and superior Faradaic efficiency for NH_3 production. The highest Faradaic efficiency of 25.9% was achieved at −0.05 V vs. RHE, while the highest ammonia yield of 25.0 $\mu g\ h^{-1}\cdot mg^{-1}_{cat}$ was obtained at −0.2 V vs. RHE. Moreover, the NRR performance of CoS/NS-G also is comparable with a high Faradaic efficiency of 15.6% at −0.05 V vs. RHE and a NH_3 yield rate of 15.7 $\mu g\ h^{-1}\cdot mg^{-1}_{cat}$ at −0.2 V vs. RHE (*SI Appendix*, Fig. S10). As shown in *SI Appendix*, Fig. S26, both of the as-obtained strongly coupled cobalt sulfide hybrids show a higher UV-vis absorption intensity at 655 nm than NS-G, suggesting a higher yield rate of NH_3 (*SI Appendix*, Fig. S11). The XPS spectra and XRD patterns of CoS_2/NS-G hybrid before and after NRR tests are shown in *SI Appendix*, Fig. S20. And, there was no change of XPS spectra XRD pattern for CoS_2/NS-G after NRR tests. Chronoamperometric experiments under Ar gas flow were also implemented and no product of NH_3 has been detected in this case (*SI Appendix*, Fig. S26). To further confirm the N source of the NH_3 during NRR process, an isotopic labeling experiment using $^{15}N_2$ as the feeding gas was performed. As shown in Fig. 4*B*, there are two peaks corresponding to $^{15}NH_4^+$ by using $^{15}N_2$ as the feeding gas, indicating that ammonia is produced via electrochemical nitrogen reduction. Moreover, three peaks corresponding to $^{14}NH_4^+$ are observed when using $^{14}N_2$ as the feeding gas and there is no detectable amount of ammonia in blank electrolyte, which further confirms that the N source of ammonia is N_2 gas. The electrolyte after different NRR durations by using $^{15}N_2$ as feeding gas was also tested by ^1H NMR. As shown in *SI Appendix*, Fig. S25, the NMR signal integrations for 40 h are almost two times the signals obtained at test for 20 h. This result demonstrated good stability of the electrocatalyst.

As shown in *SI Appendix*, Fig. S11, the strongly coupled cobalt sulfide hybrids exhibit superior NH_3 yield rate than that of the physical mixture of CoS_2 and NS-G. The above results reveal that the strongly coupled interface induced by Co–N/S–C bonds play the crucial role in enhanced NRR performance (*SI Appendix*, Fig. S21). Moreover, the overall NRR activity was also affected by the composition and distribution of cobalt sulfide nanoparticles. As shown in Fig. 4*C*, the average particle size can be tuned by using different amounts of cobalt salt. With the increasing added amount of $CoCl_2$, the particle size of CoS_2 increased. And, CoS_2/S-G exhibited the highest catalytic activity when the added amount of cobalt salt was 0.2 mmol. Notably, the strongly coupled hybrids exhibit an outstanding Faradaic efficiency and NH_3 production yield, which are superior to some reported non-noble-metal electrocatalysts (Fig. 4*D* and *SI Appendix*, Table S2). Based on the above results, the CoS_2/NS-G and CoS/NS-G hybrids have proven to be highly active NRR electrocatalysts, presenting promising potential for application in the field of N_2 fixation.

Universality of the Interfacial Engineering Strategy. The interfacial engineering strategy is general and phase selective and it can be extended to develop a series of other strongly coupled metal sulfides and graphene hybrid materials, including NiS_2/NS-G, NiS/NS-G, FeS_2/NS-G, FeS/NS-G, SnS_2/NS-G, and SnS/NS-G. Detailed characterization of these hybrid materials was performed by XRD, TEM, and XPS (*SI Appendix*, Figs. S12–S15). All of the strong coupled sulfide hybrids can be well indexed to standard metal sulfide phases, and these hybrids show the morphology of small nanoparticles homogeneously grown on a graphene nanosheet, which is similar to the morphology of the CoS_2/NS-G and CoS/NS-G materials. Moreover, according to the XPS spectra, nitrogen and sulfur have been successfully introduced into graphene nanosheet and the strong interaction between metal sulfide and graphene substrate has been constructed by the in situ annealing method. As shown in *SI Appendix*, Fig. S16, the metal disulfide hybrids exhibit a higher NH_3 yield rate than monosulfide hybrids, which suggests higher NRR electrocatalytic activity. This result reveals that the strong bridging-bonds–induced interface effect can accelerate electron transfer and plays an important part in improving electrocatalytic N_2 reduction. Thus, all of the above results confirm the universality of this interfacial engineering strategy, and this general and phase-selective synthetic method will be a promising approach for producing highly active and low-cost electrocatalysts.

Conclusion

In conclusion, we have developed an interfacial engineering strategy to design two strongly coupled cobalt-based hybrids as NRR electrocatalysts. Detailed characterization confirms that many strong Co–N/S–C bridging bonds are constructed at the interface between the metal sulfide nanoparticles and graphene support. The strongly coupled chemical bonds enable controllable interfacial effects and can accelerate the reaction kinetics by acting as an electron transport channel. As expected, the CoS_2/NS-G and CoS/NS-G hybrids exhibit excellent electrocatalytic performance for NRR with an ultrahigh Faradaic efficiency and NH_3 yield rate. This work provides a strategy to design strongly coupled hybrid materials as highly active electrocatalysts for ammonia production.

Materials and Methods

The synthetic strategy and experimental methodologies used in this work are elaborated in *SI Appendix*. These methods include the synthesis of MS_2/NS-G, MS/NS-G, and NS-G hybrid catalysts, structural characterization, and electrochemical measurements. The calculation method of NH_3 yield rate and Faradaic efficiency, product quantification, as well as $^{15}N_2$ isotope labeling experiment are also are provided in *SI Appendix*.

ACKNOWLEDGMENTS. This work was partially carried out at the University of Science and Technology of China Center for Micro and Nanoscale Research and Fabrication. This work was financially supported by the National Basic Research Program of China (Grant 2015CB932302), the Natural Science Foundation of China (Grants 21890751, 91745113, and 11621063), the National Program for Support of Top-notch Young Professionals, and the Fundamental Research Funds for the Central Universities (Grant WK 2060190084). We also appreciate the support from the Major/Innovative Program of Development Foundation of Hefei Center for Physical Science and Technology.

1. Service RF (2014) Chemistry. New recipe produces ammonia from air, water, and sunlight. *Science* 345:610.
2. Liu KH, et al. (2018) Advanced catalysts for sustainable hydrogen generation and storage via hydrogen evolution and carbon dioxide/nitrogen reduction reactions. *Prog Mater Sci* 92:64–111.
3. Kitano M, et al. (2012) Ammonia synthesis using a stable electride as an electron donor and reversible hydrogen store. *Nat Chem* 4:934–940.
4. Mehta P, et al. (2018) Overcoming ammonia synthesis scaling relations with plasma-enabled catalysis. *Nat Catal* 1:269–275.
5. Oshikiri T, Ueno K, Misawa H (2016) Selective dinitrogen conversion to ammonia using water and visible light through plasmon-induced charge separation. *Angew Chem Int Ed Engl* 55:3942–3946.
6. Lu Y, et al. (2016) Photoprompted hot electrons from bulk cross-linked graphene materials and their efficient catalysis for atmospheric ammonia synthesis. *ACS Nano* 10:10507–10515.
7. Licht S, et al. (2014) Ammonia synthesis by N_2 and steam electrolysis in molten hydroxide suspensions of nanoscale Fe_2O_3. *Science* 345:637–640.
8. Kyriakou V, Garagounis I, Vasileiou E, Vourros A, Stoukides M (2017) Progress in the electrochemical synthesis of ammonia. *Catal Today* 286:2–13.

9. Guo C, Ran J, Vasileff A, Qiao SZ (2018) Rational design of electrocatalysts and photo(electro)catalysts for nitrogen reduction to ammonia (NH_3) under ambient conditions. *Energy Environ Sci* 11:45–56.
10. van der Ham CJ, Koper MT, Hetterscheid DG (2014) Challenges in reduction of dinitrogen by proton and electron transfer. *Chem Soc Rev* 43:5183–5191.
11. Shi MM, et al. (2017) Au sub-nanoclusters on TiO_2 toward highly efficient and selective electrocatalyst for N_2 conversion to NH_3 at ambient conditions. *Adv Mater* 29: 1606550.
12. Bao D, et al. (2017) Electrochemical reduction of N_2 under ambient conditions for artificial N_2 fixation and renewable energy storage using N_2/NH_3 cycle. *Adv Mater* 29: 1604799.
13. Wang J, et al. (2018) Ambient ammonia synthesis via palladium-catalyzed electrohydrogenation of dinitrogen at low overpotential. *Nat Commun* 9:1795.
14. Shi M-M, et al. (2018) Anchoring PdCu amorphous nanocluster on graphene for electrochemical reduction of N_2 to NH_3 under ambient conditions in aqueous solution. *Adv Energy Mater* 8:1800124.
15. Kordali V, Kyriacou G, Lambrou C (2000) Electrochemical synthesis of ammonia at atmospheric pressure and low temperature in a solid polymer electrolyte cell. *Chem Commun (Camb)* 17:1673–1674.
16. Back S, Jung Y (2016) On the mechanism of electrochemical ammonia synthesis on the Ru catalyst. *Phys Chem Chem Phys* 18:9161–9166.
17. Chen S, et al. (2017) Electrocatalytic synthesis of ammonia at room temperature and atmospheric pressure from water and nitrogen on a carbon-nanotube-based electrocatalyst. *Angew Chem Int Ed Engl* 56:2699–2703.
18. Chen S, et al. (2017) Room-temperature electrocatalytic synthesis of NH_3 from H_2O and N_2 in a gas–liquid–solid three-phase reactor. *ACS Sustain Chem Eng* 5:7393–7400.
19. Furuya N, Yoshiba H (1990) Electroreduction of nitrogen to ammonia on gas-diffusion electrodes loaded with inorganic catalyst. *J Electroanal Chem Interfacial Electrochem* 291:269–272.
20. Abghoui Y, Garden AL, Howalt JG, Vegge T, Skúlason E (2016) Electroreduction of N_2 to ammonia at ambient conditions on mononitrides of Zr, Nb, Cr, and V: A DFT guide for experiments. *ACS Catal* 6:635–646.
21. Zhang X, Kong RM, Du H, Xia L, Qu F (2018) Highly efficient electrochemical ammonia synthesis via nitrogen reduction reactions on a VN nanowire array under ambient conditions. *Chem Commun (Camb)* 54:5323–5325.
22. Mukherjee S, et al. (2018) Metal-organic framework-derived nitrogen-doped highly disordered carbon for electrochemical ammonia synthesis using N_2 and H_2O in alkaline electrolytes. *Nano Energy* 48:217–226.
23. Yang X, et al. (2018) Nitrogen-doped porous carbon: Highly efficient trifunctional electrocatalyst for oxygen reversible catalysis and nitrogen reduction reaction. *J Mater Chem A* 6:7762–7769.
24. Lv C, et al. (2018) Defect engineering metal-free polymeric carbon nitride electrocatalyst for effective nitrogen fixation under ambient conditions. *Angew Chem Int Ed Engl* 57:10246–10250.
25. Lv C, et al. (2018) An amorphous noble-metal-free electrocatalyst that enables nitrogen fixation under ambient conditions. *Angew Chem Int Ed Engl* 57:6073–6076.
26. Zhu Y, et al. (2018) Structural engineering of 2D nanomaterials for energy storage and catalysis. *Adv Mater* 30:e1706347.
27. Chen P, et al. (2016) Strong-coupled cobalt borate nanosheets/graphene hybrid as electrocatalyst for water oxidation under both alkaline and neutral conditions. *Angew Chem Int Ed Engl* 55:2488–2492.
28. Tong Y, et al. (2017) A bifunctional hybrid electrocatalyst for oxygen reduction and evolution: Cobalt oxide nanoparticles strongly coupled to B,N-decorated graphene. *Angew Chem Int Ed Engl* 56:7121–7125.
29. Su H, et al. (2017) Activating cobalt nanoparticles via the Mott-Schottky effect in nitrogen-rich carbon shells for base-free aerobic oxidation of alcohols to esters. *J Am Chem Soc* 139:811–818.
30. Zhu H, et al. (2015) When cubic cobalt sulfide meets layered molybdenum disulfide: A core-shell system toward synergetic electrocatalytic water splitting. *Adv Mater* 27: 4752–4759.
31. Cai P, Huang J, Chen J, Wen Z (2017) Oxygen-containing amorphous cobalt sulfide porous nanocubes as high-activity electrocatalysts for the oxygen evolution reaction in an alkaline/neutral medium. *Angew Chem Int Ed Engl* 56:4858–4861.
32. Liu H, et al. (2017) Electronic structure reconfiguration toward pyrite NiS_2 via engineered heteroatom defect boosting overall water splitting. *ACS Nano* 11:11574–11583.
33. Chen P, et al. (2017) Enhanced catalytic activity in nitrogen-anion modified metallic cobalt disulfide porous nanowire arrays for hydrogen evolution. *ACS Catal* 7: 7405–7411.
34. Luo P, et al. (2017) Targeted synthesis of unique nickel sulfide (NiS, NiS_2) microarchitectures and the applications for the enhanced water splitting system. *ACS Appl Mater Interfaces* 9:2500–2508.
35. Chen P, et al. (2017) Atomically dispersed iron-nitrogen species as electrocatalysts for bifunctional oxygen evolution and reduction reactions. *Angew Chem Int Ed Engl* 56: 610–614.
36. Gao S, et al. (2015) Transformation of worst weed into N-, S-, and P-tridoped carbon nanorings as metal-free electrocatalysts for the oxygen reduction reaction. *J Mater Chem A* 3:23376–23384.
37. Bi E, et al. (2014) A quasi core–Shell nitrogen-doped graphene/cobalt sulfide conductive catalyst for highly efficient dye-sensitized solar cells. *Energy Environ Sci* 7: 2637–2641.
38. Jia Y, et al. (2016) Defect graphene as a trifunctional catalyst for electrochemical reactions. *Adv Mater* 28:9532–9538.
39. Liu W, et al. (2016) A highly active and stable hydrogen evolution catalyst based on pyrite-structured cobalt phosphosulfide. *Nat Commun* 7:10771.
40. Chen CJ, et al. (2015) An integrated cobalt disulfide (CoS_2) co-catalyst passivation layer on silicon microwires for photoelectrochemical hydrogen evolution. *J Mater Chem A* 3:23466–23476.
41. Sarret G, et al. (1999) Chemical forms of sulfur in geological and archeological asphaltenes from Middle East, France, and Spain determined by sulfur K- and L-edge X-ray absorption near-edge structure spectroscopy. *Geochim Cosmochim Acta* 63:3767–3779.
42. Zheng Y, et al. (2014) Hydrogen evolution by a metal-free electrocatalyst. *Nat Commun* 5:3783.
43. Liang Y, et al. (2011) Co_3O_4 nanocrystals on graphene as a synergistic catalyst for oxygen reduction reaction. *Nat Mater* 10:780–786.